Nuclear Inst, and Methods in Physics Research B 423 (2018) 27–36

Contents lists available at ScienceDirect

Nuclear Inst. and Methods in Physics Research B

journal homepage: www.elsevier.com/locate/nimb

Measurement of the neutron angular distribution from a beryllium target bombarded with a 345-MeV/u ^{238}U beam at the RIKEN RI beam factory

Noriaki Nakao[a,*], Yoshitomo Uwamino[b], Kanenobu Tanaka[b]

[a] Institute of Technology, Shimizu Corporation, Tokyo, Japan
[b] RIKEN Nishina Center, Wako, Saitama, Japan

ARTICLE INFO

Keywords:
Neutron
^{238}U beam
Activation detector
Bismuth
Angular distribution
Monte Carlo

ABSTRACT

The angular distribution of neutrons produced from a 4-mm-thick beryllium target bombarded with a 345-MeV/u ^{238}U beam was measured outside the target chamber using bismuth and aluminum activation detectors at angles of 4.5°, 10°, 30°, 60°, 70° and 90° from the beam axis. Following two hours of irradiation and photo-peak analyses, the production rates of the radionuclides were obtained for the ^{209}Bi(n,xn)$^{210-x}$Bi(x = 4–12) and ^{27}Al(n,α)^{24}Na reactions. Using the Particle and Heavy Ion Transport code System (PHITS), a Monte Carlo simulation of the production rates was performed and the ratios of the calculated to the experimental results (C/E) ranged from 0.6 to 1.0 generally and 0.4 to 1.3 in worst cases.

1. Introduction

A number of high-power accelerators are under construction for use in radioisotope beam facilities. To ensure radiation safety in such facilities, secondary neutron data due to beam irradiation play an important role in predicting activation and prompt-radiation levels.

Measurements of neutrons produced from targets bombarded by heavy ions in the energy range of 100–800 MeV per nucleon (MeV/u) have been conducted at the Heavy Ion Medical Accelerator in Chiba (HIMAC) at the National Institute of Radiological Sciences, Japan [1,2,3,4,5]. In the experiment procedure, the angular distributions of neutron-energy spectra were measured according to the time-of-flight (TOF) method using an NE213 organic-liquid scintillator with heavy ions of helium, carbon, neon, silicon, argon, iron, and xenon. However, ions heavier than xenon are unavailable in accelerated beams at HIMAC. On the contrary, at the Gesellschalt für Schwerionenforschung (GSI) in Germany, neutron-energy spectra from an iron target bombarded with a 1 GeV/u ^{238}U beam have been measured in the forward direction [6]. Nevertheless, this type of experimental data for very-heavy ions such as ^{238}U beams is very scarce.

Since 2007, the Radioactive Isotope Beam Factory (RIBF) at RIKEN has supplied ^{238}U beams at energies of approximately 350 MeV/u to a target in the Big RIKEN Projectile-fragment Separator (BigRIPS) [7]. In this facility, neutron and photon distributions around the BigRIPS separator are measured for a ^{238}U beam using activation detectors [8] and thermoluminescent dosimeters (TLD) [9]. Owing to the difficulty of conducting TOF measurements arising from the lack of sufficient space for long flight paths, passive detectors, such as activation detectors, are useful for measuring radiation fields in narrow regions or gaps in actual accelerator components. To obtain benchmark experimental data for the secondary neutrons produced from a target impacted by a ^{238}U beam, measurement using activation detectors placed at several locations outside the target chamber was performed in this study.

2. Experiment

Fig. 1 shows the experimental setup at the target chamber made of aluminum and the Superconducting Triplet Quadrupole (STQ) magnet at BigRIPS. A 4-mm-thick beryllium target was equipped inside the chamber. The target was struck by a 345-MeV/u ^{238}U beam. On bombarding the target, the ^{238}U ion of the beam is separated in-flight into fission products of neutron-rich unstable nuclei at intermediate masses, and secondary neutrons are emitted during the reaction at the same time. The ^{238}U beam penetrating the target at a forward angle, together with the radioisotopes (RIs) generated, pass through the hole of a copper beam scraper followed by the STQ magnet and are transported downstream, as indicated in the Fig. 1. Due to proprietary technology, the detailed structure of the STQ magnet is not shown in the figure. Essential materials used in the experimental setup are listed in Table 1.

Neutron measurements using the activation detectors were performed parasitically with the RI-beam experiments. To measure secondary neutrons from the target, activation-detector samples of bismuth and aluminum were placed outside of the chamber and the STQ magnet at angles of 4.5°, 10°, 30°, 60°, 70° and 90° from the beam line,

* Corresponding author at: 3-4-17, Etchujima, Koto-ku, Tokyo 135-8530, Japan.
E-mail address: noriaki.nakao@shimz.co.jp (N. Nakao).

https://doi.org/10.1016/j.nimb.2018.02.036
Received 30 October 2017; Received in revised form 28 February 2018; Accepted 28 February 2018
Available online 15 March 2018
0168-583X/

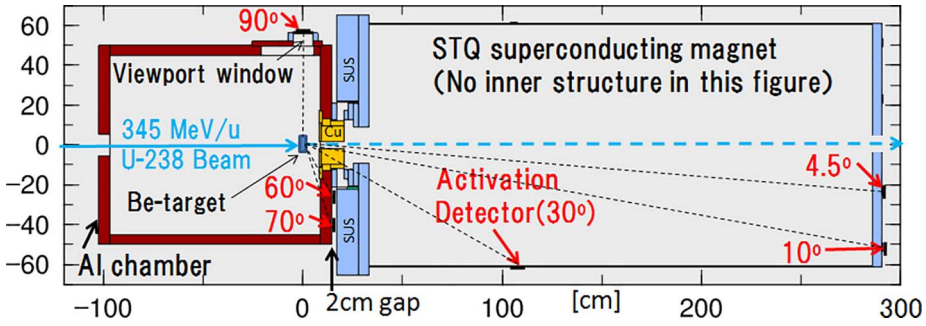

Fig. 1. Horizontal cross-section of the target chamber and the STQ magnet. "SUS" indicates stainless steel. The detailed structure of the STQ magnet is not shown due to proprietary technology.

Table 1
Essential materials used in experimental setup.

Equipment	Material
Aluminum target chamber	A5052
Copper beam scraper	C1100
Tungsten shield	AN1800
Stainless-steel shield	SUS304
STQ vacuum chamber	SUS304

as shown in Fig. 1. Therefore, neutrons after collision with surrounding materials, such as the chamber and the STQ magnet, were included in the data measured by the activation detectors. Two sample sizes, ϕ40-mm × 4-mm and ϕ20-mm × 2-mm, were used for both bismuth and aluminum to cross-check the results to identify differences caused by different sizes and efficiencies. The samples at 4.5° and 10° were placed on the rear surface of the STQ magnet, as shown in Fig. 2. The samples at 30° were placed on the side wall of the STQ magnet. The samples at 60° and 70° were placed in the gap between the target chamber and the STQ magnet. For easy handling of the samples, they were stuck on the carton board, as shown in the left photo of Fig. 3, and the board was inserted into the gap with a sponge spacer, as shown in the right photo of Fig. 3. The samples at 90° were placed on the glass of the viewport window.

The average intensity of the ^{238}U beam for the 2-h irradiation period was approximately 7.2 × 10^{10} s^{-1} (~11.5 particle nanoamperes) with a 20% uncertainty in the beam-monitor. Fig. 4 presents the beam-intensity history during the 2-h irradiation and demonstrates that it was almost stable. The relative beam-intensity-fluctuation history was obtained by detection of recoil protons generated at the target with using coincidence measurement of three plastic scintillators. The absolute beam intensity is periodically calibrated with a beam-current measurement by the Faraday cup.

The beam was stopped for a while before and after the irradiation period to set up and remove the activation samples in the corresponding locations. After irradiation, the activation detectors were removed from the irradiation places, and the energy spectra of photons from radionuclides generated by ^{209}Bi(n,xn)$^{210-x}$Bi(x = 4–12) and ^{27}Al(n,α)^{24}Na reactions were measured using a high-purity germanium-semiconductor detector (Ge detector) (type:GC2019, Mirion Technologies (Canberra) KK). Fig. 5 shows an example of the measured energy spectrum. Table 2 gives the analyzed radionuclide-production reactions, half-lives and photon energies. Photo-peak counts were obtained for the corresponding photon energies by summing up the peak regions and subtracting the baseline contribution, which was estimated for both sides as shown in Fig. 6. The peak counts, S, and their standard deviations, σ, were estimated by the following equation:

$$S = N_p - b_1 N_1 - b_2 N_2 \quad (1)$$

$$\sigma = \sqrt{N_p + \beta_1^2 N_1 + \beta_2^2 N_2} \quad (2)$$

$\beta_1 = 0.5W_p/W_1$ and $\beta_2 = 0.5W_p/W_2$. N_p, N_1, and N_1 are the gross counts in the peak region, baseline region 1, and baseline region 2, respectively; W_p, W_1, and W_2 are channel widths for the peak region, baseline region 1, and baseline region 2, respectively.

Fig. 7(a) shows a photon measurement by the Ge detector with a uniformly activated volume sample. As standard photon sources calibrated in the same-volume samples of bismuth and aluminum were not available, a standard mixed-radionuclide point source was directly placed on the acrylic plate or on the non-irradiated samples of the activation detectors for measuring the efficiency as shown in Fig. 7 (b). The photo-peak efficiencies of the Ge detector for corresponding gamma-ray energies were estimated by electrons and photon simulations using the MCNP5 Monte Carlo code [10], considering the self-

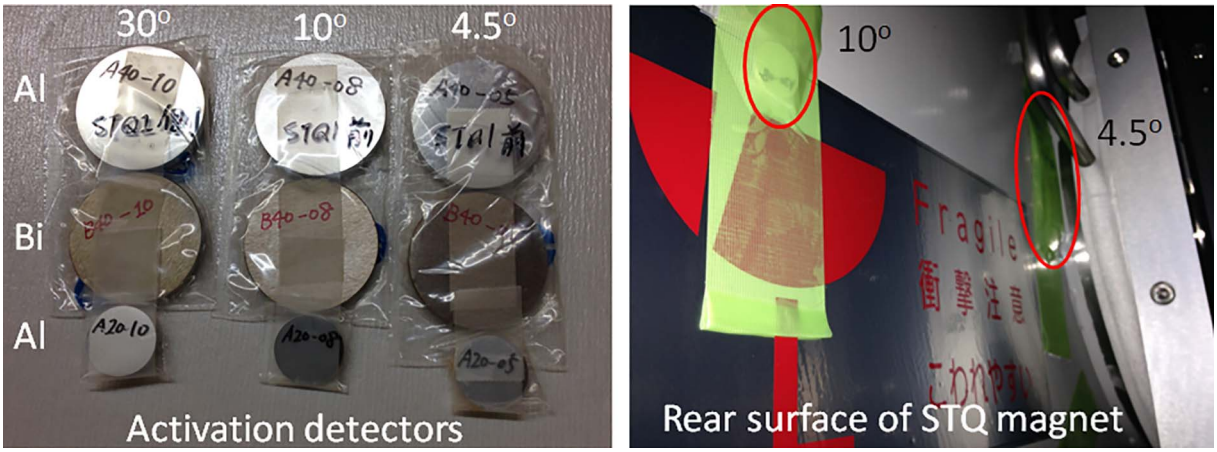

Fig. 2. Photos of activation-detector samples at 4.5°, 10° and 30° and the situation of attached samples on the rear surface of the STQ magnet.